Photoluminescence of excitons bound to the isoelectronic hydrogen-related defects B^1_{71} (1.1377 eV) in silicon

A. S. Kaminskii and E. V. Lavrov
Institute of Radioengineering and Electronics, Russian Academy of Sciences, 11 Mohovaya Street, Moscow, 103907, Russia

V. A. Karasyuk and M. L. W. Thewalt
Department of Physics, Simon Fraser University, Burnaby, British Columbia, Canada V5A 1S6
(Received 8 March 1994)

Photoluminescence (PL) spectra of excitons bound to the isoelectronic defects B^1_{71} (1.137 68 eV principal no-phonon line) created in phosphorus-doped silicon grown in a hydrogen atmosphere as a result of irradiation by thermal neutrons were investigated in magnetic fields up to 12 T and under uniaxial stress. The C_{3V} symmetry of these defects was determined unambiguously from the dependences of the Zeeman splitting and the intensities of spectral components on magnetic-field orientation. The ground state of the bound exciton is split into a doublet with approximately 30 μeV energy separation. This splitting, which is not evident in the zero-field spectra because of the selection rules, results in the appearance of an additional spectral component in a magnetic field. Using group theoretical methods we constructed a Hamiltonian for excitons bound to the B^1_{71} isoelectronic center, which takes into account electron-hole coupling and interaction with external perturbations. The phenomenological parameters of this Hamiltonian were determined from the optimal fit between theoretical and experimental dependences of the PL peak positions and their amplitudes on magnetic field and uniaxial stress. The proposed model of these bound excitons explains all of our experimental observations.

I. INTRODUCTION

Investigations of the recombination luminescence of excitons bound to radiation-damage defects in semiconductors provides valuable information about these defects. The isoelectronic center B^1_{71} is one of the three radiation damage defects recently discovered[1] in phosphorous-doped silicon grown in a hydrogen atmosphere which bind excitons with equal thermal and optical dissociation energies. This kind of isoelectronic center has been less extensively studied than bound excitons (BE's) with optical dissociation energies, which are considerably greater than their thermal dissociation energies, (the latter are usually referred to as "pseudodonors" or "pseudoacceptors"). Recently, Safonov and Lightowlers[2] have demonstrated that the center B^1_{71} incorporates two hydrogen atoms in nonequivalent positions. However, the symmetry and details of the structure of B^1_{71} have not been determined. Kaminskii, Safonov, and Lavrov[1] found several excited electronic states of BE's associated with B^1_{71} which can control the BE lifetime and its temperature dependence, because electron-hole recombination in the ground state is partially forbidden. The goal of the present work was to investigate the symmetry of B^1_{71} isoelectronic centers, to characterize the ground and the excited electronic states of corresponding BE's, and to furnish a model describing electron-hole coupling accounting for the energy-level structure of these BE's using perturbation photoluminescence (PL) spectroscopy and methods of group theory.

II. EXPERIMENTAL TECHNIQUE

We studied the samples of phosphorus-doped ($N_P = 2\times10^{14}$ cm^{-3}) silicon grown in a hydrogen atmosphere by the floating-zone technique. The samples were irradiated with a beam of thermal neutrons at a dose of 10^{17} cm^{-2}, corresponding to a transmutational phosphorus content of 2×10^{13} cm^{-3} (the cadmium number $K=200$). The irradiated samples were isothermally annealed for 30 min in a muffle furnace at the annealing temperature of 460–470 °C depending on the sample origin.

The uniaxial stress technique developed in Ref. 3 was used to achieve the best stress homogeneity. For that purpose the samples were cut in a form of parallelepipeds with dimensions $2\times2\times20$ mm^3 with rectangular pyramids on the ends. The samples were x-ray oriented in ⟨001⟩, ⟨111⟩, and ⟨110⟩ crystallographic directions. The ends of the pyramids were positioned in the centers of conical holes stamped in the brass pistons to which force was applied by a push rod with weights on the top. The stress rig with the sample was placed either into a variable temperature He cryostat with temperature set in the range between 5 and 20 K or into an immersion He cryostat. 0.3 W cw radiation from a Ti-sapphire laser (Spectra Physics) tuned to 80 μ wavelength was used to photoexcite the samples. Linear splitting of the no-phonon line α_1 of excitons bound to neutral phosphorus donors was used for the precise stress calibration.

The Zeeman effect measurements were performed in liquid He with the sample in the two inch bore of a 12 T superconducting solenoid (Oxford Instruments). The sample orientation could be changed accurately between ⟨001⟩ and ⟨110⟩ in a $(1\bar{1}0)$ crystallographic plane by rotating the sample around its $\langle 1\bar{1}0\rangle$ axis which was perpendicular to the magnetic field. PL radiation emitted from the sample perpendicular to the field (Voigt configuration) was collected by a system of mirrors, col-

limated by a lens, and analyzed using Fourier-transform interferometer (BOMEM DA8) fitted with a cooled $In_xGa_{1-x}As$ photo diode at spectral resolutions of up to 0.025 cm^{-1}.

III. RESULTS AND DISCUSSION

The samples subject to no external perturbation show at 17 K four strong features in near band gap PL spectra (Fig. 1), X^1_{71} at 9176.29 cm^{-1}, X^1_{68} at 9178.87 cm^{-1}, X^1_{60} at 9185.48 cm^{-1}, and X^1_{57} at 9187.9 cm^{-1} where the labels are those introduced by Kaminskii, Safanov, and Lavrov[1] The amplitude ratios of these four features depend on the sample temperature but do not change from sample to sample, which implies that all four components are due to the same center, namely B^1_{71}. The amplitudes of X^1_{60} and X^1_{57} are comparable with those of X^1_{71} and X^1_{68} only above 10 K, and are vanishingly small at 4.2 K. The spectrum is dominated by the transitions X^1_{71} and X^1_{68} which arise from the first two excited states of B^1_{71}, because the optical transition from the ground state is partially forbidden;[1] as a consequence PL intensity increases dramatically when the temperature is raised from 1.6 to 10 K. Our uniaxial stress and Zeeman effect measurements were designed in order to determine the symmetry of excitons bound to B^1_{71} and thus to help determine the structure of this defect.

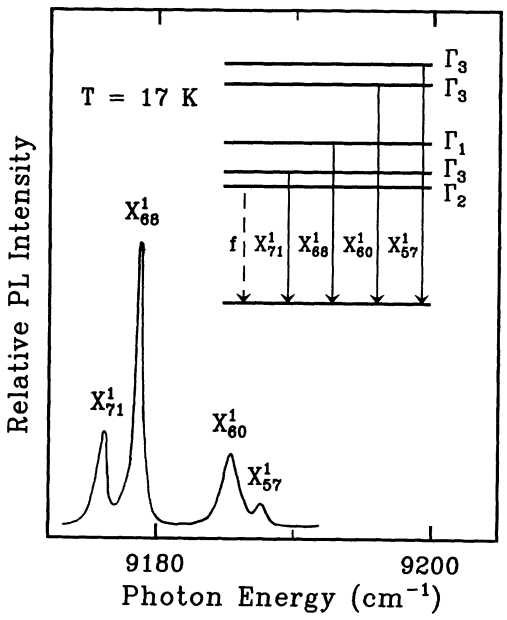

FIG. 1. A photoluminescence (PL) spectrum of excitons bound to the B^1_{71} centers taken at 17 K without external perturbation of the sample. We employ the labeling scheme from Ref. 1. Upper-case letters X label observed spectral components with subscripts and superscripts showing the energy separation of a given spectral feature from the free exciton (FE) no-phonon (NP) edge. For example, X^1_{68} is 16.8 meV below the FE, etc. The inset shows the energy levels of the bound excitons on B^1_{71} labeled by corresponding irreducible representations in the notation of Koster *et al.* (Ref. 4) and possible optical transitions to the ground state of the center B^1_{71}. f stands for the forbidden optical transition from the state Γ_2 to the state Γ_1.

A. The Zeeman effect measurements

Figure 2 shows the evolution of PL spectra of excitons bound to the B^1_{71} defects in a weak magnetic field with ⟨001⟩ orientation. In Fig. 2, the spectra recorded at (a) 0, (b) 0.25, and (c) 0.50 T are shown by solid lines. Dots and dashed lines represent experimental and calculated PL peak positions, respectively. The spectra were recorded at a low temperature of 2 K when the lines X^1_{60} and X^1_{57} vanish. In a magnetic field the line X^1_{68} remains unsplit (component 4) at an approximately constant position while the line X^1_{71} splits into two components, 2 and 3. One more component, 1, appears in a magnetic field with the amplitude increasing rapidly when the field intensity increases from 0 to 0.5 T. This component is absent at zero field, indicating that the corresponding dipole optical transition is prohibited.

When the field is increased up to 12 T, components 2, 3, and 4 thermalize and only component 1 remains in the PL spectra at low temperatures. Figure 3 shows the dependences of the peak positions on the magnetic field with ⟨001⟩, ⟨111⟩, and ⟨110⟩ orientations in the range 0–12 T. For the magnetic field orientations other than ⟨001⟩ the number of spectral components is greater than four, with two components evolving from the lowest zero-field energy level of the BE. Only these two components remain in the spectra at low temperatures in a strong magnetic field. This doublet splitting of the low-energy component in a magnetic field is due to the different possible orientations of the defect with respect to the magnetic field. The absence of this orientational

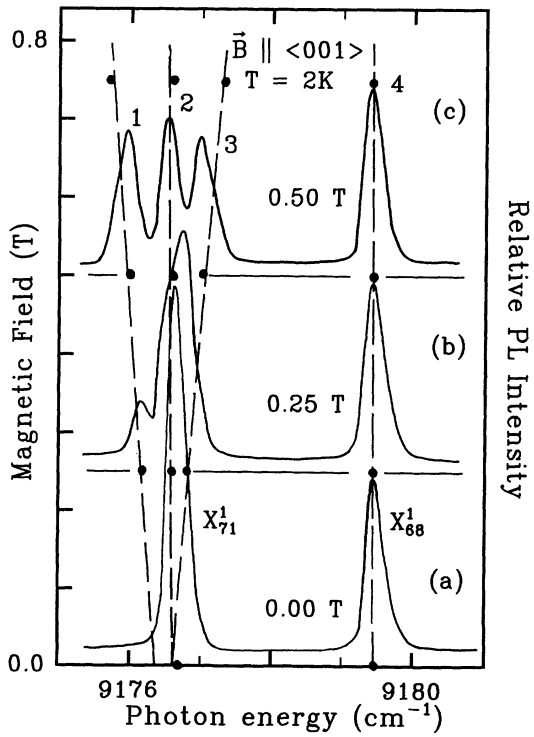

FIG. 2. NP PL spectra of BE's on B^1_{71} in a weak ⟨001⟩ magnetic field at 2 K and (a) 0.0 T, (b) 0.25 T, (c) 0.50 T (Voigt configuration). Dashed lines show calculated and dots show experimental peak positions as a function of the magnetic field.

splitting for magnetic fields with ⟨001⟩ orientation indicates that all the B^1_{71} centers are oriented equivalently with respect to the ⟨001⟩ crystallographic axis, therefore, the B^1_{71} radiation damage defect has trigonal symmetry with the main axis oriented along one of the equivalent ⟨111⟩ crystallographic directions.

B. Theoretical model of excitons bound to B^1_{71} center

The results of the Zeeman effect measurements can be explained by a simple model in which the defect has a C_{3V} symmetry with the main threefold rotation axis aligned with one of the equivalent ⟨111⟩ crystallographic directions. The defect potential with such a symmetry should split the fourfold degenerate hole state derived from the top of the valence band into two doublets, Γ_4 and $(\Gamma_5+\Gamma_6)$ (in the notation of Koster *et al.*[4]). It may also combine the six electron states associated with the six conduction band minima into the valley-orbit combinations with the valley-orbit splitting onto four energy levels, ground state Γ_1 and excited states $2\Gamma_3$ and Γ_1 (electron spin is not taken into account because of the negligible spin-orbit interaction). Throughout this paper, we will assume that the electron occupies the ground state Γ_1 (Γ_4 if spin is taken into account) with energy separation from the excited electron states exceeding significantly any other splitting of the BE energy levels.

The hole states will be expanded in the orthonormal basis:

$$\phi_1=\frac{1}{\sqrt{2}}(|3/2;3/2\rangle-i|3/2;-3/2\rangle)\ ,$$

$$\phi_2=\frac{1}{\sqrt{2}}(-i|3/2;3/2\rangle+|3/2;-3/2\rangle)\ ,$$

$$\phi_3=|3/2,+1/2\rangle\ ,\quad \phi_4=|3/2,-1/2\rangle\ ,$$

where $|3/2,m\rangle, m=\pm 3/2,\pm 1/2$, represent the canonical basis for the angular momentum $j=3/2$. The functions ϕ_1 and ϕ_2 form the bases of the group C_{3V} irreducible representations Γ_5 and Γ_6, respectively, and the functions ϕ_3 and ϕ_4 form the basis of the Γ_4 representation. Coupling of the hole in the BE with the electron spin transforming as Γ_4 results in the splitting into five energy levels $(\Gamma_4+\Gamma_5+\Gamma_6)^h\otimes\Gamma_4^e=\Gamma_1+\Gamma_2+3\Gamma_3$ (Fig. 1). The final state transforms according to the unit representation Γ_1; as a consequence, at zero magnetic field the dipole optical transitions from the state Γ_2 of the BE are prohibited. We assume that the state Γ_2 is the ground state of the BE, because the PL peaks associated with the ground state in a magnetic field disappear at zero field. We also assume that the BE states derived from the hole states ϕ_1 and ϕ_2, $(\Gamma_5+\Gamma_6)^h\otimes\Gamma_4^e=2\Gamma_3$ correspond to the lines X^1_{60} and X^1_{57} and, therefore, have significantly higher energy than the states derived from the hole states ϕ_3 and ϕ_4, $\Gamma_4^h\otimes\Gamma_4^e=\Gamma_1+\Gamma_2+\Gamma_3$. The latter give rise to the lines X^1_{71} and X^1_{68}. The Zeeman splitting is small if compared with the splitting between the pairs of components X^1_{60}, X^1_{57} and X^1_{71}, X^1_{68}; therefore, we can neglect the coupling between the BE states with the hole ϕ_3,ϕ_4 and the states with the hole ϕ_1,ϕ_2 in our interpretation of the Zeeman effect.

Therefore, we assume that at zero field the ground state of the BE incorporates the hole occupying the states Γ_4 with the approximate angular momentum projections on the defect axis $m_j=\pm 1/2$. Interaction of the hole in this state with the electron in the state Γ_4 splits the ground state of the BE into three substates $\Gamma_4^h\otimes\Gamma_4^e=\Gamma_2+\Gamma_3+\Gamma_1$. Dipole optical transitions from the state Γ_2 to the ground state of the defect Γ_1 are prohibited, therefore, only two spectral components X^1_{71} and X^1_{68} corresponding to states of the BE associated with the Γ_4 hole state can be observed in the zero-field PL spectrum (the bottom spectrum in Fig. 2). However, when a magnetic field is applied, the symmetry of the system is reduced still further and dipole optical transitions from the states evolving from the zero-field state Γ_2 become allowed. Correspondingly, additional components associated with this state appear in the spectra (component 1 in Fig. 2) with the amplitude growing rapidly when the magnetic field is increased from 0 to 0.5 T. In magnetic fields with ⟨001⟩ orientation, the zero-field BE state Γ_3 splits into a doublet (components 2 and 3) and the state Γ_1 remains unsplit (component 4). When the field is increased further, components 3 and 4 anticross in accordance with theoretical predictions (Fig. 3). Thus the evolution of the PL spectra in a magnetic field, which is shown in Figs. 2 and 3, provides reliable identification of the zero-field BE energy levels.

The Hamiltonian of a BE in a magnetic field

$$H=H^0+H(\mathbf{B})\ , \tag{2}$$

where H^0 is the zero-field Hamiltonian and $H(\mathbf{B})$ describes the interaction with the magnetic field, can be presented as a 4×4 matrix in the basis of the products $\phi_m\zeta_p$, where ϕ_m, $m=3,4$, and ζ_p, $p=1,2$, form the single-hole and single-electron bases, correspondingly, with quantization axis aligned with the defect. We constructed this matrix from symmetry considerations using the method of invariants of Bir and Pikus.[5] The zero-field Hamiltonian H^0 can be expressed in a form of the linear combination

$$H^0=\Delta_1(\sigma_0\otimes\sigma_0)+\Delta_2(\sigma_z\otimes\sigma_z)+\Delta_3(\sigma_x\otimes\sigma_x+\sigma_y\otimes\sigma_y)\ , \tag{3}$$

where σ_x, σ_y, and σ_z are the Pauli matrices, σ_0 is the 2×2 unit matrix, and the phenomenological interaction constants Δ_1, Δ_2, and Δ_3 define the zero-field energy levels of BE

$$\begin{aligned} E(\Gamma_1)&=\Delta_1-\Delta_2-2\Delta_3\ ,\\ E(\Gamma_2)&=\Delta_1-\Delta_2+2\Delta_3\ ,\\ E(\Gamma_3)&=\Delta_1+\Delta_2\ . \end{aligned} \tag{4}$$

Equation (4) in combination with the zero-field positions of the lines X^1_{71}, X^1_{68} and the extrapolated zero-field posi-

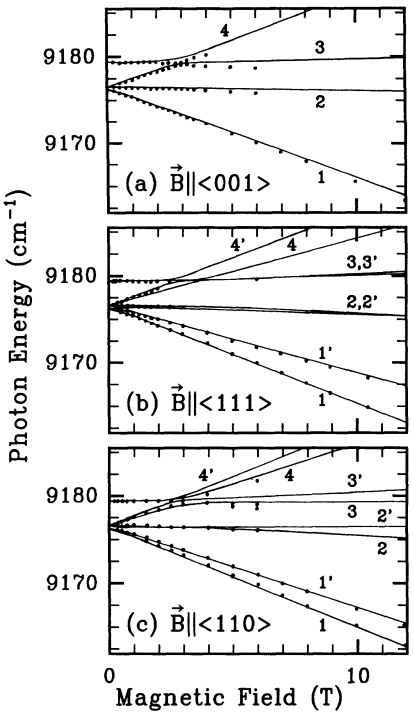

FIG. 3. Dependences of the PL peak positions on a magnetic field with (a) ⟨001⟩, (b) ⟨111⟩, and (c) ⟨110⟩ orientations. Dots show the experiment and solid lines show the theory.

tion of component 1 in Fig. 2 gives immediately the values of the constants $\Delta_1=9276.88$ cm^{-1}, $\Delta_2=-0.59$ cm^{-1}, and $\Delta_3=-0.73$ cm^{-1}.

The Hamiltonian of the interaction with the magnetic field can be expressed in a similar manner as the linear combination

$$H(\mathbf{B})=\tfrac{1}{2}\mu_B\left\{g^e\sum_{i=x,y,z}B_i(\sigma_0\otimes\sigma_i)+g_{\parallel}^h B_z(\sigma_z\otimes\sigma_0)+g_{\perp}^h[B_x(\sigma_x\otimes\sigma_0)+B_y(\sigma_y\otimes\sigma_0)]\right\}, \quad (5)$$

where μ_B is the Bohr magneton, and $g_{\parallel}^h=1.3$ and $g_{\perp}^h=2.88$ are the hole g factors which were determined from the best fit to experimental data (Fig. 3). We assume that the electron can be characterized by a single isotropic g factor $g^e=2.0$.

In order to verify that the center B_{71}^1 has C_{3V} symmetry we have recorded the Zeeman spectra at constant fields of 6 and 12 T with the sample orientation changing gradually between ⟨001⟩ and ⟨111⟩ in a (110) plane. The angular dependences of the peak positions and amplitudes at 12 T are presented in Fig. 4, where the solid lines represent the results of calculations based on the model described above. As one can see, the patterns of these angular dependences are in good agreement with experimental data. These patterns depend on the symmetry of the center and on the ratio $r=g_{\parallel}^h/g_{\perp}^h$ (Fig. 5), therefore, they enable identification of the point group of the defect.

Any defect in a cubic crystal belongs to one of the five crystal classes: triclinic, monoclinic, trigonal, tetragonal, or rhombic. The crystal class uniquely defines the pat-

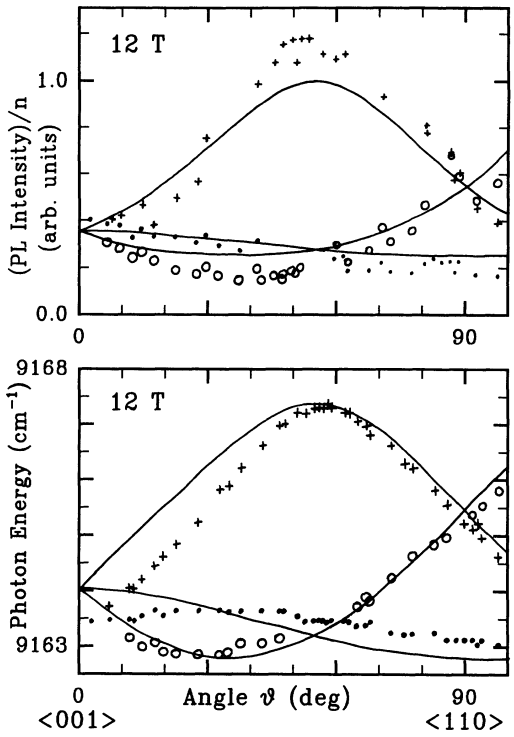

FIG. 4. Zeeman splitting of the ground state of BE's on the centers B_{71}^1 (bottom) and amplitudes of corresponding spectral components (top) as measured from the PL spectra at 12 T in a magnetic field with different orientations. Dots, circles, and pluses represent experiment, solid lines represent theory. θ is the angle between the magnetic field and the ⟨001⟩ crystallographic direction. The $(1\bar{1}0)$ crystallographic plane is parallel to the magnetic field. The splitting is due to the different possible orientations of the defects B_{71}^1 with respect to the magnetic field. n is the orientational degeneracy of the corresponding PL component.

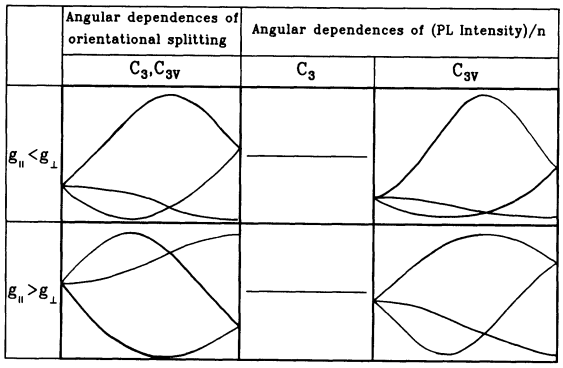

FIG. 5. Predicted angular dependences of the ground-state orientational splitting and of the PL peak intensities in a magnetic field for BE's on isoelectronic centers with C_3 or C_{3V} symmetry. The $(1\bar{1}0)$ crystallographic plane is parallel to the magnetic field. The angle θ between magnetic field and the ⟨001⟩ crystallographic direction increases from the left- to the right-hand side of each diagram.

tern of the angular dependence of the orientational splitting in magnetic fields. However, this dependence alone does not uniquely define the point group of the defect. For instance, a trigonal defect in silicon may have one of the two point groups C_3 or C_{3V} (Ref. 6). In both cases the angular dependence of the orientational splitting will have the same pattern (Fig. 5). For instance, the center responsible for the lines $J_1,\ldots,J_5$ observed by Sauer and Weber[7] in phosphorus-doped Si irradiated with neutrons must have a trigonal symmetry and $g_{\parallel}^h < g_{\perp}^h$ according to the angular dependence observed by Sauer and Weber for the splitting of the line J_1 in a magnetic field. We found that the point group of the defect can be determined unambiguously from the angular dependence of the peak amplitudes if $g_{\parallel}^h \neq g_{\perp}^h$. This dependence can be calculated by evaluating the dipole momentum operator matrix elements on the set of proper linear combinations of $\phi_m \zeta_p$ which diagonalize the Hamiltonian (2). In doing so it is important to take into account properly the degeneracies of corresponding eigenstates. The results of these calculations for the center with C_3 or C_{3V} symmetry and $g_{\parallel}^h < g_{\perp}^h$ or $g_{\parallel}^h > g_{\perp}^h$ are summarized in Fig. 5. We assumed in our calculations that in a zero magnetic field, dipole transition probabilities are the same for every state in the triplet. We believe that this is also the case for the centers I_2 (Ref. 7). From the comparison of Figs. 4 and 5 it is obvious that the center B_{71}^1 has a C_{3V} symmetry. It is remarkable that in this case when $g_{\parallel}^h < g_{\perp}^h$ the angular dependences of the peak positions and amplitudes look qualitatively the same. In our opinion the method described above can be used for the point-group identification of other defects as well.

C. Uniaxial stress measurements

Interpretation of our uniaxial stress experiments requires taking into account the hole states Γ_5 and Γ_6, because under large uniaxial stress these states mix with the states Γ_4. Thus we have to construct the Hamiltonian

$$H = H^0 + H(\sigma_{kl}) , \tag{6}$$

where σ_{kl} is the stress tensor and $H(\sigma_{kl})$ describes the influence of stress on BE states, in the full basis of eight functions

$$\Psi_{mp} = \phi_m \zeta_p \quad (m = 1,\ldots,4 \text{ and } p = 1,2) . \tag{7}$$

We have constructed a Hamiltonian (6) using the method of invariants of Bir and Pikus[5] from sixteen linearly independent matrices, A_1^1, A_1^2, A_1^3, A_2^1, A_2^2, A_2^3, E_x^1, E_x^2, E_x^3, E_x^4, E_x^5, E_y^1, E_y^2, E_y^3, E_y^4, and E_y^5 shown in Appendix A, which transform as partners in the basis ϕ_m according to irreducible representations of the group C_{3V} and the Pauli matrices σ_x, σ_y, σ_z, and the 2×2 unit matrix σ_0 in the basis ζ_p representing the electron. The 8×8 zero stress Hamiltonian matrix H^0 has the form

$$\begin{aligned} H^0 = {} & \Delta_1(A_1^1 \otimes \sigma_0) + \Delta_2(A_2^1 \otimes \sigma_z) + \Delta_3(E_x^1 \otimes \sigma_x + E_y^1 \otimes \sigma_y) \\ & + \Delta_4(A_1^2 \otimes \sigma_0) + \Delta_5(A_2^2 \otimes \sigma_z) \\ & + \Delta_6(E_x^4 \otimes \sigma_x + E_y^4 \otimes \sigma_y) , \end{aligned} \tag{8}$$

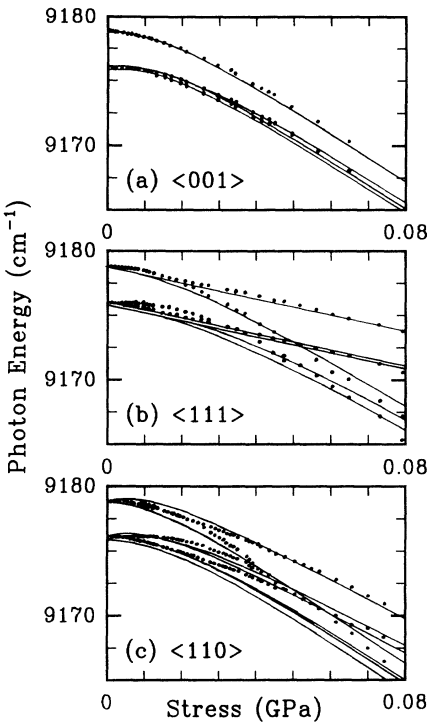

FIG. 6. Peak positions as a function of uniaxial stress in (a) ⟨001⟩, (b) ⟨111⟩, and (c) ⟨110⟩ orientations. Dots represent experiment and solid curves represent theory.

with phenomenological electron-hole interaction constants Δ_1, Δ_2, and Δ_3 the same as in Eq. (3), Δ_6 set to zero, and $\Delta_4 = 11.21$ cm^{-1}, $\Delta_5 = 1.21$ cm^{-1} as found from the best fit to the experiment (Fig. 6). The stress Hamiltonian matrix $H(\sigma_{kl})$ has the form

$$\begin{aligned} H(\sigma_{kl}) = {} & \delta_1 \sigma_{zz}(A_1^1 \otimes \sigma_0) + \delta_2(\sigma_{xx} + \sigma_{yy})(A_1^1 \otimes \sigma_0) \\ & + \delta_3 \sigma_{zz}(A_1^2 \otimes \sigma_0) + \delta_4(\sigma_{xx} + \sigma_{yy})(A_1^2 \otimes \sigma_0) \\ & + \delta_5(\sigma_{xy} E_x^2 \otimes \sigma_0 + 1/2(\sigma_{xx} - \sigma_{yy}) E_y^2 \otimes \sigma_0) \\ & + \delta_6(\sigma_{xz} E_x^3 \otimes \sigma_0 + \sigma_{yz} E_y^3 \otimes \sigma_0) , \end{aligned} \tag{9}$$

with phenomenological constants $\delta_1 = 7.7$ meV/GPa, $\delta_2 = -9.8$ meV/GPa, $\delta_3 = 17.3$ meV/GPa, $\delta_4 = -18.2$ meV/GPa, $\delta_5 = \pm 47.5$ meV/GPa, and $\delta_6 = \pm 27.5$ meV/GPa, as determined from the best fit with the experiment (Fig. 6). For generality we have constructed also the Hamiltonian $H(\mathbf{B})$ of the interaction with a magnetic field in the full basis (7) which is shown in the Appendix B. As one can see, the proposed model for BE's associated with the isoelectronic centers B_{71}^1 can explain all experimental observations.

ACKNOWLEDGMENTS

The authors wish to thank Dr. N. S. Averkiev for fruitful discussions. This work was supported partly by the Natural Science and Engineering Research Council of Canada, by the International Science Foundation Long Term Research Grant, and by an INTAS Grant.

APPENDIX A

The following matrices were constructed in the basis of functions ϕ_m (1) and they transform as partners according to irreducible representations Γ_i of the point group C_{3V}. A plus or minus in the parentheses indicates even (+) or odd (−) parity with respect to time inversion.

Γ_1:

$$A_1^1=\sigma_2\otimes\sigma_0 \quad (+),$$

$$A_1^2=\sigma_1\otimes\sigma_0 \quad (+),$$

$$A_1^3=\sigma_1\otimes\sigma_z \quad (-).$$

Γ_2:

$$A_2^1=\sigma_2\otimes\sigma_z \quad (-),$$

$$A_2^2=\sigma_1\otimes\sigma_y \quad (-),$$

$$A_2^3=\sigma_1\otimes\sigma_x \quad (-).$$

Γ_3:

$$E_x^1=\sigma_2\otimes\sigma_x \quad (-), \quad E_y^1=\sigma_2\otimes\sigma_y \quad (-),$$

$$E_x^2=\sigma_x\times(\sigma_y+\sigma_z) \quad (+),$$

$$E_y^2=\sigma_x\otimes\sigma_x+\sigma_y\otimes\sigma_0 \quad (+),$$

$$E_x^3=\sigma_x\otimes\sigma_x-\sigma_y\otimes\sigma_0 \quad (+),$$

$$E_y^3=\sigma_x\times(\sigma_z-\sigma_y) \quad (+),$$

$$E_x^4=\sigma_x\otimes\sigma_0+\sigma_y\otimes\sigma_x \quad (-),$$

$$E_y^4=\sigma_y\otimes(\sigma_z-\sigma_y) \quad (-),$$

$$E_x^5=\sigma_y\otimes(\sigma_y+\sigma_z) \quad (-),$$

$$E_y^5=\sigma_y\otimes\sigma_x-\sigma_x\otimes\sigma_0 \quad (-),$$

$$\sigma_1=\begin{bmatrix}1 & 0\\ 0 & 0\end{bmatrix}, \quad \sigma_2=\begin{bmatrix}0 & 0\\ 0 & 1\end{bmatrix}.$$

APPENDIX B

In the basis of eight functions $\Psi_{mp}=\phi_m\xi_p$ (7) ($m=1,\ldots,4;p=1,2$) the Hamiltonian of the interaction with the magnetic field has the form

$$\begin{aligned}H(\mathbf{B})=\tfrac{1}{2}\mu_B\{&g^e_{\parallel(1/2)}B_z(A_1^2\otimes\sigma_z)+g^e_{\perp(1/2)}[B_x(A_1^1\otimes\sigma_x)+B_y(A_1^1\otimes\sigma_y)]+g^h_{\parallel(1/2)}B_z(A_2^1\otimes\sigma_0)\\&+g^h_{\perp(1/2)}[B_x(E_x^1\otimes\sigma_0)+B_y(E_y^1\otimes\sigma_0)]+g^e_{\parallel(3/2)}B_z(A_1^2\otimes\sigma_z)\\&+g^e_{\perp(3/2)}[B_x(A_1^2\otimes\sigma_x)+B_y(A_1^2\otimes\sigma_y)]+g^h_{\parallel(3/2)}B_z(A_2^2\otimes\sigma_0)+g^h_{\perp(3/2)}[G_x(E_x^4\otimes\sigma_0)+B_y(E_y^4\otimes\sigma_0)]\},\end{aligned}$$

where μ_B is the Bohr magneton, and the g factors $g^e_{\parallel(1/2)}$, $g^e_{\perp(1/2)}$, $g^h_{\parallel(1/2)}$, $g^h_{\perp(1/2)}$, $g^e_{\parallel(3/2)}$, $g^e_{\perp(3/2)}$, $g^h_{\parallel(3/2)}$, and $g^h_{\perp(3/2)}$ can be determined from comparison with experiment.

[1]A. S. Kaminskii, A. N. Safonov, and E. V. Lavrov, Fiz. Tverd. Tela Leningrad **33**, 859 (1991) [Sov. Phys. Solid State **33**, 488 (1991)].

[2]V. A. Karasyuk, A. G. Steele, A. Mainwood, E. C. Lightowlers, G. Davies, D. M. Brake, and M. L. W. Thewalt, Phys. Rev. B **45**, 11 736 (1992).

[3]A. S. Kaminskii, V. A. Karasyuk, and Ya. E. Pokrovskii, Zh. Eksp. Teor. Fiz. **83**, 2237 (1982) [Sov. Phys. JETP **56**, 1295 (1982)].

[4]G. F. Koster, J. O. Dimmock, R. G. Wheeler, and H. Statz, *Properties of the Thirty-two Point Groups* (MIT Press, Cambridge, MA, 1966).

[5]G. L. Bir and G. E. Pikus, *Simmetrya i Deformatsionnye Effecty v Poluprovodnikakh* (Izdatel'stvo "Nauka," Moscow, 1972 [*Symmetry and Strain-Induced Effects in Semiconductors* (Halsted, New York, 1974)].

[6]A. A. Kaplyuansky, Opt. Spectrosc. **16**, 329 (1964).

[7]R. Sauer and J. Weber, Physica **116B**, 195 (1983).